EFFECT OF ASPECT RATIOS ON LONGITUDINAL AND LATERAL MOTIONS OF UNMANNED AERIAL VEHICLE

E. J. Abdullah, M. R. Ajir , M. T. Ahmad and M. N. Filipski,.
Aerospace Engineering Department, Universiti Putra Malaysia, Serdang, Selangor, Malaysia
Email: ermira@eng.upm.edu.my

ABSTRACT

The study of wing with varying aspect ratio is critical in the development of the morphing wing for Unmanned Aerial Vehicle (UAV). A morphing wing permits a change in the camber, aspect ratio, wing twist and wing sweep while simultaneously supporting structural wing loads. UAV with this wing design will be able to carry out multiple objectives mission. This paper investigates the effect of aspect ratio on the stability of the longitudinal and lateral motions of UAV. The poles of the motion are calculated and root locus for the motions are plotted to validate that the variable aspect ratio (VAR) wings sustain stability during symmetric changes in wing span. Preliminary study on the stability of a generic UAV shows that it remains stable for values of aspect ratio from 3 to 10.

Key words: *Aspect Ratio, Stability, Flight Dynamics, UAV, Longitudinal Motion, Lateral Motion.*

INTRODUCTION

In recent years there has been a great interest in developing Unmanned Aerial Vehicle (UAV) for surveillance and reconnaissance purposes. UAV typically has low aspect ratio wing and fly at low Reynolds number compared to full-scale aircraft, so subsequently this generate a pressing need to understand the dynamics and stability of UAV. As a reaction to this, studies on the effects of aspect ratio on the aerodynamics, performance and stability of UAVs have been carried out to verify the feasibility of the morphing wing design [1 – 7]. This paper presents the results of a study which emphasizes on the longitudinal and lateral stabilities for a predefined range of aspect ratio.

High aspect ratio wing and low aspect ratio wing have different aerodynamic properties and thus aircraft wings with different aspect ratio will not exhibit similar aircraft performance. Low aspect ratio wing have poor aerodynamic efficiency L/D at low speeds and in addition to that it is dynamically unstable. However, it has a very high angle of attack of stall. On the other hand, high aspect ratio wing is more stable but its angle of attack of stall is not as high.

Typically, a high aspect ratio wing is used for low speed flight. This is meant to reduce the induced drag which is the drag created from the generation of lift by wings or a lifting body during flight. Wing with high aspect ratio produces small vortices, in comparison with wing with low aspect ratio. The use of larger aspect ratio is a way to reduce the induced drag. However, UAVs usually have a low aspect ratio, so it is crucial to find out the effects of these wings at low Reynolds number. A lot of work has been carried out in trying to model the nonlinear lift of low aspect ratio wing mathematically. However, only recently research on the experimental investigation of low aspect ratio has been conducted by Torres and Mueller [3]. The research focuses on the small air vehicles operating at low Reynolds number. Wind tunnel testing was performed on wing planforms of four different geometries. Aerodynamics analysis of the low aspect ratio wing at low Reynolds numbers was presented as a result of this research.

The investigation of wing with varying aspect ratios is most critical in the development of the pneumatic morphing aspect ratio wing done by Blondeau and Pines[1]. A pneumatic telescopic wing permits a change in the aspect ratio while simultaneously supporting structural wing loads. UAV with this wing design will be able to carry out multiple objectives mission.

EQUATIONS OF MOTION

Longitudinal Equations of Motion

The longitudinal motion of an airplane is characterized by two types of oscillatory modes of motion. The modes are long-period or phugoid mode and short-period mode. Phugoid mode is lightly damped and has a long period. Short period mode is heavily damped and has a very short-period, hence the name.

According to Nelson [8], the linearized longitudinal set of equations are given as follows

$$
\begin{aligned}
&(\frac{d}{dt} - X_u)\Delta u - X_w \Delta w + (g\cos\theta_0)\Delta\theta = X_\delta \Delta\delta + X_{\delta_T}\Delta\delta_T \\
&- Z_u \Delta u + [(1 - Z_{\dot{w}})\frac{d}{dt} - Z_w]\Delta - [(u_0 + Z_q)\frac{d}{dt} - g\sin\theta_0]\Delta\theta = Z_\delta \Delta\delta + Z_{\delta_T}\Delta\delta_T \qquad (1) \\
&- M_u \Delta u - (M_{\dot{w}}\frac{d}{dt} + M_w)\Delta w + \frac{d^2}{dt^2} - M_q \frac{d}{dt})\Delta\theta = M_{\delta_T} + M_{\delta_T}\Delta\delta_T
\end{aligned}
$$

where $\Delta\delta$ and $\Delta\delta_T$ are the aerodynamics and propulsive controls respectively.

The force derivatives Zq and $Z_{\dot{w}}$ usually are negligible, so we can simplify the above equations and rewrite them in the state space form which yields

$$
\begin{bmatrix} \Delta\dot{u} \\ \Delta\dot{w} \\ \Delta\dot{q} \\ \Delta\dot{\theta} \end{bmatrix} = \begin{bmatrix} X_u & X_w & 0 & -g \\ Z_u & Z_w & u_0 & 0 \\ M_u + M_w Z_u & M_w + M_{\dot{w}} Z_w & M_q + M_{\dot{w}} u_0 & 0 \\ 0 & 0 & 1 & 0 \end{bmatrix} \begin{bmatrix} \Delta u \\ \Delta w \\ \Delta q \\ \Delta\theta \end{bmatrix}
$$

$$
+ \begin{bmatrix} X_\delta & X_{\delta_T} \\ Z_\delta & Z_{\delta_T} \\ M_\delta + M_{\dot{w}} Z_\delta & M_{\delta_T} + M_{\dot{w}} Z_{\delta_T} \\ 0 & 0 \end{bmatrix} \begin{bmatrix} \Delta\delta \\ \Delta\delta_T \end{bmatrix} \qquad (2)
$$

The phugoid mode is characterized by changes in the pitch attitude, altitude and velocity at a nearly constant angle of attack. An approximation of the phugoid mode can be obtained by neglecting the pitching moment equation and assuming that the change in the angle of attack is 0. By making this assumptions the homogeneous longitudinal state equations reduce to:

$$
\begin{bmatrix} \Delta\dot{u} \\ \Delta\dot{\theta} \end{bmatrix} = \begin{bmatrix} X_u & -g \\ \dfrac{-Z_u}{u_0} & 0 \end{bmatrix} \begin{bmatrix} \Delta u \\ \Delta\theta \end{bmatrix} \qquad (3)
$$

The eigenvalues of the phugoid approximation are acquired by solving the following equation

$$
|\lambda I - A| = 0 \qquad (4)
$$

By expanding the determinant, we obtain the phugoid poles

$$\lambda_p = \left[X_u \pm \sqrt{X_u^2 + 4\frac{Z_u g}{u_0}} \right] \Big/ 2.0 \tag{5}$$

Finally, the frequency and damping ratio can be expressed as

$$\omega_{n_p} = \sqrt{\frac{-Z_u g}{u_0}} \tag{6}$$

$$\zeta_p = \frac{-X_u}{2\omega_{n_p}} \tag{7}$$

The short-period approximation is given to be

$$\begin{bmatrix} \Delta\dot{\alpha} \\ \Delta\dot{q} \end{bmatrix} = \begin{bmatrix} \frac{Z_\alpha}{u_0} & 1 \\ M_\alpha + M_{\dot{\alpha}}\frac{Z_\alpha}{u_0} & M_q + M_{\dot{\alpha}} \end{bmatrix} \begin{bmatrix} \Delta\alpha \\ \Delta q \end{bmatrix} \tag{8}$$

The eigenvalues can be obtained by solving the following equation

$$\left|\lambda I - A\right| = 0 \tag{9}$$

By expanding the determinant, we will obtain the short-period poles

$$\lambda_{sp} = \left(M_q + M_{\dot{\alpha}} + \frac{Z_\alpha}{u_0} \right) \Big/ 2 \pm \left[\left(M_q + M_{\dot{\alpha}} + \frac{Z_{\dot{\alpha}}}{u_0} \right)^2 - 4\left(M_q \frac{Z_\alpha}{u_0} - M_\alpha \right) \right]^{1/2} \Big/ 2 \tag{10}$$

And in terms of frequency and damping ratio,

$$\omega_{n_{sp}} = \left[\left(M_q \frac{Z_\alpha}{u_0} - M_\alpha \right) \right]^{1/2} \tag{11}$$

$$\zeta_{sp} = -\left[M_q + M_{\dot{\alpha}} + \frac{Z_\alpha}{u_0} \right] \Big/ (2\omega_{n_{sp}}) \tag{12}$$

Lateral-Directional Equations of Motion

The roots to the lateral-directional characteristic equation are composed of two real roots and a pair of complex roots. A slowly convergent or divergent motion is called the spiral mode. A highly convergent motion is called the rolling mode. A lightly damped oscillatory motion with a low frequency is called the Dutch roll mode.

According to Nelson [8], the lateral-directional equations of motion consist of the side force, rolling moment and yawing moment equations of motion. The lateral set of equations is given as follow:

$$\left(\frac{d}{dt}-Y_v\right)\Delta v - Y_p\Delta p + (u_0 - Y_r)\Delta r - g\cos\theta_0\Delta\phi = Y_{\delta_r}\Delta\delta_r$$
$$-L_v\Delta v + \left(\frac{d}{dt}-L_p\right)\Delta p - \left(\frac{I_{xz}}{I_z}\frac{d}{dt}+L_r\right)+\Delta r = L_{\delta_a}\Delta\delta_a + L_{\delta_r}\Delta\delta_r \tag{13}$$
$$-N_v\Delta v - \left(\frac{I_{xz}}{I_z}\frac{d}{dt}+N_p\right)\Delta p + \left(\frac{d}{dt}-N_r\right)\Delta r = N_{\delta_a}\Delta\delta_r$$

By rearranging and collecting like terms, the above equations can be stated in state variable form:

$$\begin{bmatrix}\Delta\dot{\beta}\\ \Delta\dot{p}\\ \Delta\dot{r}\\ \Delta\dot{\phi}\end{bmatrix} = \begin{bmatrix} \frac{Y_\beta}{u_0} & \frac{Y_p}{u_0} & -(1-\frac{Y_r}{u_0}) & \frac{g\cos\theta_0}{u_0}\\ L_\beta & L_p & L_r & 0\\ N_\beta & N_p & N_r & 0\\ 0 & 1 & 0 & 0\end{bmatrix}\begin{bmatrix}\Delta\beta\\ \Delta p\\ \Delta r\\ \Delta\phi\end{bmatrix}$$
$$+\begin{bmatrix} 0 & \frac{Y_\beta}{u_0}\\ L_{\delta_a} & L_{\delta_r}\\ N_{\delta_a} & N_{\delta_r}\\ 0 & 0\end{bmatrix}\begin{bmatrix}\Delta\delta_a\\ \Delta\delta_r\end{bmatrix} \tag{14}$$

The spiral mode is caused by the changes in the bank angle φ and the heading angle ψ. The aerodynamics contributions due to β and r are usually on the same order of magnitude. The characteristic root which gives the spiral root is

$$\lambda_{spiral} = \frac{L_\beta N_r - L_r N_\beta}{L_\beta} \tag{15}$$

The roll motion can be approximated by the single degree of freedom of rolling motion. The roll root is given by,

$$\lambda_{roll} = -\frac{1}{\tau} = L_p \tag{16}$$

In order to obtain the Dutch roll mode approximation, we can consider that it consists only of sideslipping and yawing motions, therefore we can neglect the rolling moment equation. The approximation will be:

$$\begin{bmatrix}\Delta\dot{\beta}\\ \Delta\dot{r}\end{bmatrix} = \begin{bmatrix}\frac{Y_\beta}{u_0} & -\left(1-\frac{Y_r}{u_0}\right)\\ N_\beta & N_r\end{bmatrix}\begin{bmatrix}\Delta\beta\\ \Delta r\end{bmatrix} \tag{17}$$

The Dutch roll roots can be obtained by solving the characteristic equation

$$\lambda^2 - \left(\frac{Y_\beta + u_0 N_r}{u_0}\right)\lambda + \frac{Y_\beta N_r - N_\beta Y_r + u_0 N_\beta}{u_0} = 0 \tag{18}$$

We can also determine the undamped natural frequency and damping ratio

$$\omega_{n_{DR}} = \sqrt{\frac{Y_\beta N_r - N_\beta Y_r + u_0 N_\beta}{u_0}} \tag{19}$$

$$\zeta_{DR} = -\frac{1}{2\omega_{n_{DR}}}\left(\frac{Y_\beta + u_0 N_r}{u_0}\right) \tag{20}$$

DYNAMICS STABILITY

One of many possible definitions of dynamic stability for nonlinear systems is given in terms of the eigenvalues of the Jacobian matrix,

$$A = \begin{bmatrix} \frac{\partial g_1}{\partial x_1} & \frac{\partial g_1}{\partial x_2} \\ \frac{\partial g_2}{\partial x_1} & \frac{\partial g_2}{\partial x_2} \end{bmatrix} \tag{21}$$

If all the eigenvalues of A has a negative real parts we say that the reference solution, (x_R, u_R), is stable. If atleast one of the eigenvalue of A has a positive real part we say that the reference solution, (x_R,u_R), is unstable. If atleast one eigenvalues of A has a zero real part, and if all the other eigenvalues have negative real parts, we can draw no conclusion about the stability of the reference solution. The neutral stability of the origin implies all solutions are bounded. Instability of the origin implies the system has some unbounded solutions.

ROOT LOCUS

Root locus is a graphical presentation of the closed loop poles as the system parameter is varied. It is a powerful method of analysis and design for stability and transient response. It gives the qualitative description of a control system's performance. The root locus can be used to solve first- and second-order systems, its strength is in the ability to provide solution for systems of order higher than two. The root locus can be used in the process of designing a control system. It allows the designer to view the movement of the poles of the closed loop transfer function as system parameters are varied.

The properties of the root locus can be derived from the general control system where the closed-loop transfer function for the system is

$$T(s) = \frac{KG(s)}{1 + KG(s)H(s)} \tag{22}$$

A pole, s, exists when the characteristic polynomial in the denominator becomes zero. If any pole lie on the left half portion of the complex plane is stable which means the response decays with time. The $j\omega$-axis crossing is a point on the root locus that separates the stable operation of the system from the unstable operation.

METHODOLOGY

In this study the Predator was chosen as the test vehicle. Table 1 shows the basic specifications of the UAV. The aspect ratio of the model was varied from 1 – 10, while all other parameters were kept constant. However those parameters which are affected by the change of aspect ratio such as wing span, and wing surface area, were also changed accordingly.

Table 1: Basic Specifications of Predator

Parameter	Value
Weight	3900 lbf
Fuselage Length	25 ft
Mean Aerodynamic Chord of Wing	5.0625
Body Size Area	64.674 ft^2
Thickness to Chord Ratio of Wing	0.1467
Thickness to Chord Ratio of Horizontal Tail	0.0909
Horizontal Tail Span	12.5 ft
Surface Area of Horizontal Tail	27.5 ft^2
Chord of Rudder	0.694
Mean Aerodynamic Chord of Vertical Tail	0.97225
Trim Velocity	158 knots
Mach Number	0.3382

In total 10 test cases for the UAV were set up, and for each case the equations of motion was developed. The poles were calculated for each test case. The longitudinal equations of motion give the phugoid and short period poles. The lateral equations of motion give poles for the spiral, roll and dutch roll motion.

RESULTS AND ANALYSIS

Result of Poles with Increasing Aspect Ratio

From the calculation, the phugoid poles remain stable for all values of aspect ratio as shown in Table 2. Phugoid poles become less negative, meaning less stable, when the value of aspect ratio increases from 1 to 4. However, the poles become more negative, which means more stable when the value of aspect ratio is increased from 4 to 10. The phugoid poles are most stable when aspect ratio is 1 and least stable when aspect ratio is 5.

Table 2: Results for Phugoid Poles with Increasing Aspect Ratio (AR)

AR	Poles
1	-0.029622 ± 0.16002i
2	-0.019971 ± 0.16641i
3	-0.016638 ± 0.16717i
4	-0.015682 ± 0.16688i
5	-0.01582 ± 0.16641i
6	-0.016527 ± 0.16592i
7	-0.017563 ± 0.16546i
8	-0.018777 ± 0.16501i
9	-0.020174 ± 0.16456i
10	-0.021663 ± 0.16412i

From the calculation, the short period poles remain stable for all values of aspect ratio as shown in Table 3. Short period poles become more negative, which means more stable when the value of aspect ratio is increased from 1 to 10. The short period poles are most stable when aspect ratio is 10 and least stable when aspect ratio is 1.

Table 3: Results for Short Period Poles with Increasing Aspect Ratio (AR)

AR	Poles
1	-4.2131 ± 6.9482i
2	-4.2949 ± 6.0089i
3	-4.398 ± 6.3235i
4	-4.5024 ± 6.8666i
5	-4.6051 ± 7.4461i
6	-4.7056 ± 8.0092i
7	-4.8054 ± 8.5421i
8	-4.9065 ± 9.0317i
9	-5.0111 ± 9.5121i
10	-5.1104 ± 9.9614i

From the calculation, the spiral mode pole is stable only when aspect ratio is 1 or 2. The pole becomes unstable when the aspect ratio is increased from 3 to 10 as shown in Table 4. The pole becomes more unstable when the aspect ratio is decreased from 2 to 1. The pole becomes more unstable when the aspect ratio decreases from 10 to 3. The short period pole is most stable when aspect ratio is 1 and least stable when aspect ratio is 3. An unstable spiral mode may result in a turning flight trajectory. However, this problem can be rectified by increasing the dihedral effect or yaw damping to make the spiral mode more stable.

Table 4: Results for Spiral Mode Poles with Increasing Aspect Ratio (AR)

AR	Poles
1	-0.03802
2	-0.11207
3	0.095206
4	0.06364
5	0.05173
6	0.046196
7	0.044431
8	0.042499
9	0.040646
10	0.038489

From the calculation, the roll mode pole is unstable only when aspect ratio is 1 or 2. The pole becomes stable when the aspect ratio is increased from 3 to 10 as shown in Table 5. The poles become more unstable when the aspect ratio is decreased from 2 to 1. The pole becomes more stable when the aspect ratio increases from 3 to 10. The short period pole is most stable when aspect ratio is 10 and least stable when aspect ratio is 1.

Table 5: Results for Roll Mode Poles with Increasing Aspect Ratio (AR)

AR	Poles
1	0.3166
2	0.14713
3	-0.19968
4	-0.34069
5	-0.57998
6	-0.94215
7	-1.3995
8	-1.9658
9	-2.669
10	-3.4799

From the calculation, the dutch roll mode poles remain stable for all values of aspect ratio as shown in Table 6. Dutch roll mode poles become less negative, meaning less stable, when the value of aspect ratio increases from 1 to 9. However, the poles become more negative, which means more stable when the value of aspect ratio is increased from 9 to 10. The dutch roll mode poles are most stable when aspect ratio is 1 and least stable when aspect ratio is 9.

Table 6: Results for Dutch Roll Mode Poles with Increasing Aspect Ratio (AR)

AR	Poles
1	-0.88112 ± 2.7682i
2	-0.50401 ± 2.6615i
3	-0.38524 ± 2.4227i
4	-0.3278 ± 2.2665i
5	-0.29443 ± 2.1544i
6	-0.26828 ± 2.0792i
7	-0.24337 ± 2.0381i
8	-0.22219 ± 2.0346i
9	-0.21882 ± 2.0582i
10	-0.23695 ± 2.1028i

Root Locus for Longitudinal Motion

Figures 1 to 10 show the root locus plot for the longitudinal motion. Each plot contains the short period poles, phugoid poles and zeros. The root locus remains on the left half portion of the complex plane for all values of aspect ratio, which means that the system is stable.

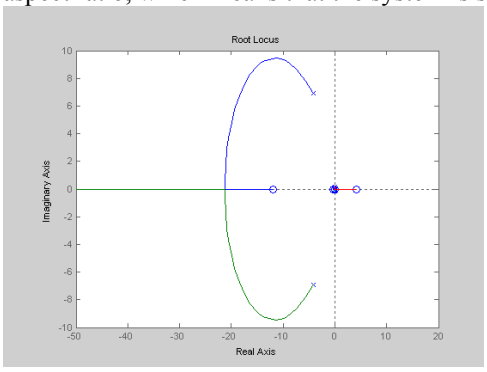

Figure 1 : Root Locus of Longitudinal Motion for AR = 1

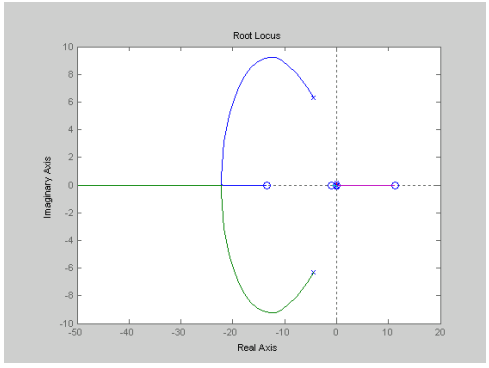

Figure 2 : Root Locus of Longitudinal Motion for AR = 2

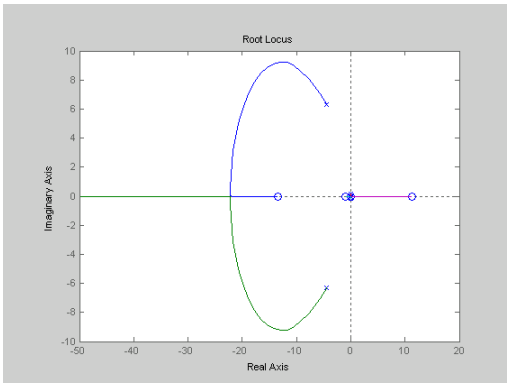

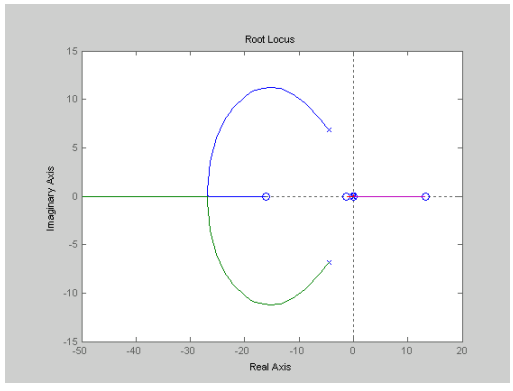

Figure 3 : Root Locus of Longitudinal Motion for AR = 3

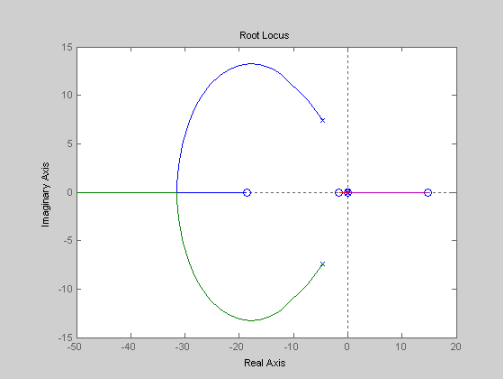

Figure 4 : Root Locus of Longitudinal Motion for AR = 4

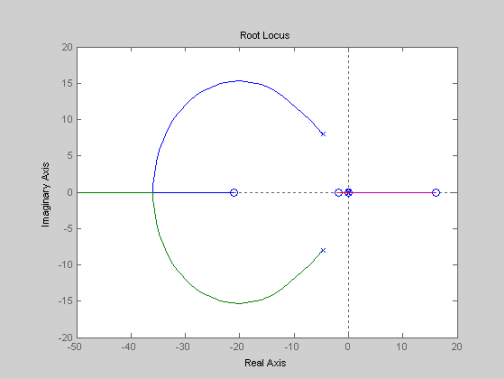

Figure 5 : Root Locus of Longitudinal Motion for AR = 5

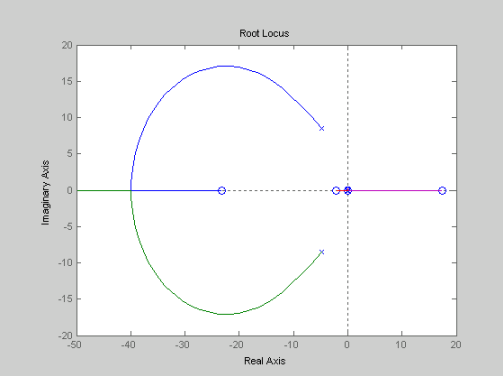

Figure 6 : Root Locus of Longitudinal Motion for AR = 6

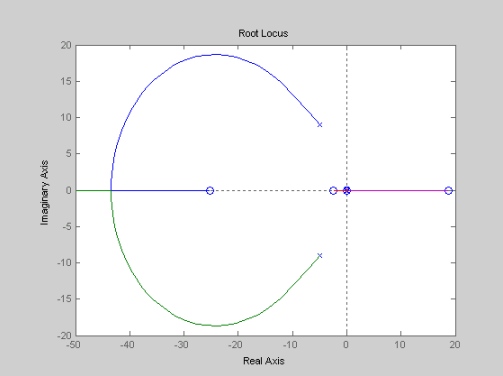

Figure 7 : Root Locus of Longitudinal Motion for AR = 7

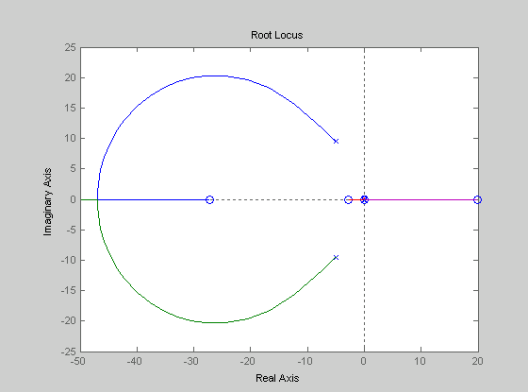

Figure 8 : Root Locus of Longitudinal Motion for AR = 8

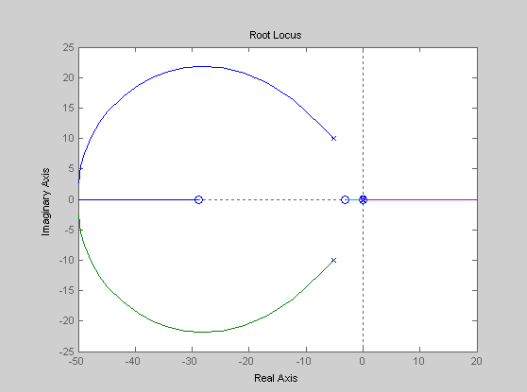

Figure 9 : Root Locus of Longitudinal Motion for AR = 9

Figure 10 : Root Locus of Longitudinal Motion for AR = 10

Root Locus for Lateral Motion

Figures 1 to 10 show the root locus plot for the lateral motion. Each plot contains the spiral mode pole, roll mode pole, dutch roll mode poles and zeros. The root locus remains on the left half portion of the complex plane for all values of aspect ratio, which means that the system is stable.

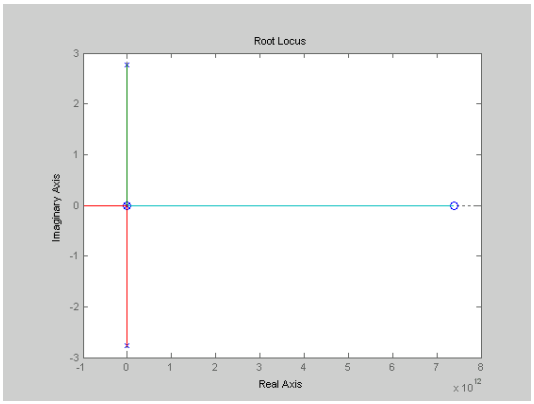

Figure 1 : Root Locus of Longitudinal Motion for AR = 1

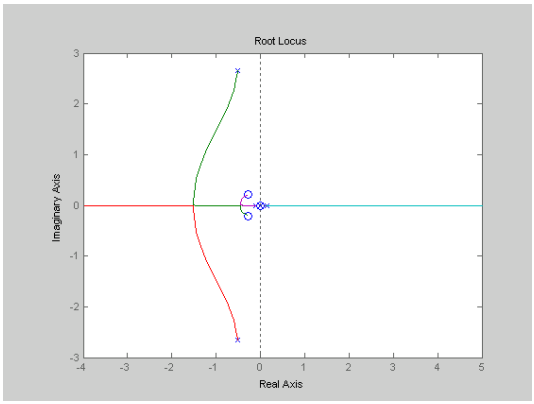

Figure 2 : Root Locus of Longitudinal Motion for AR = 2

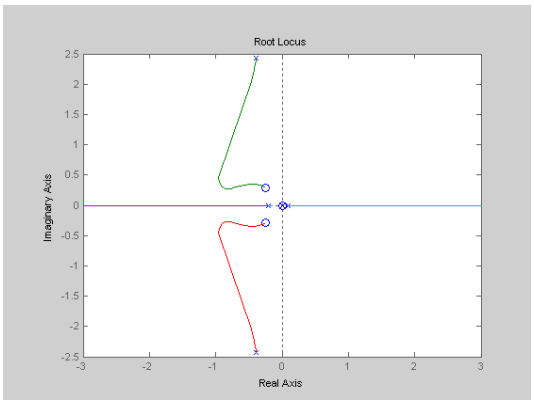

Figure 3 : Root Locus of Longitudinal Motion for AR = 3

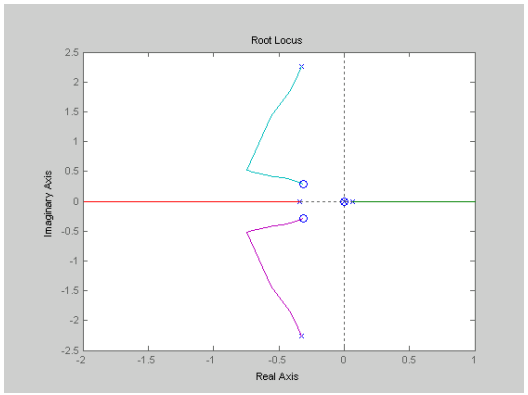

Figure 4 : Root Locus of Longitudinal Motion for AR = 4

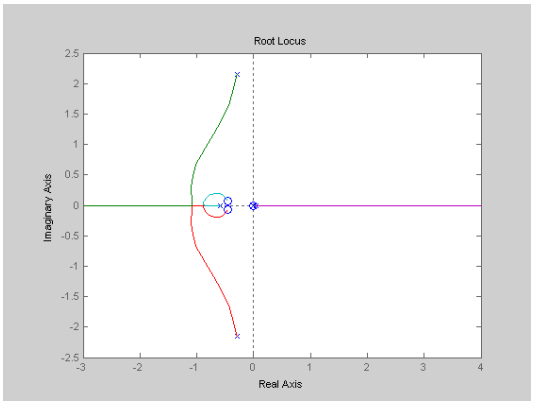

Figure 5 : Root Locus of Longitudinal Motion for AR = 5

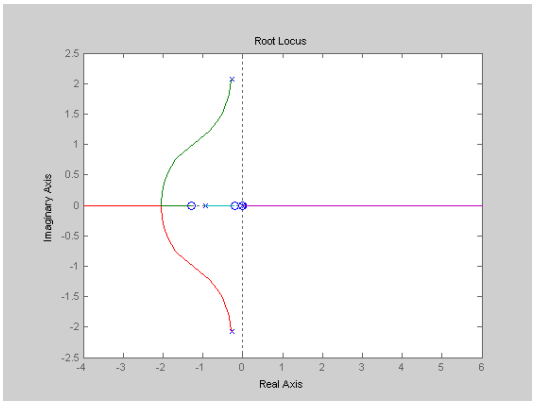

Figure 6 : Root Locus of Longitudinal Motion for AR = 6

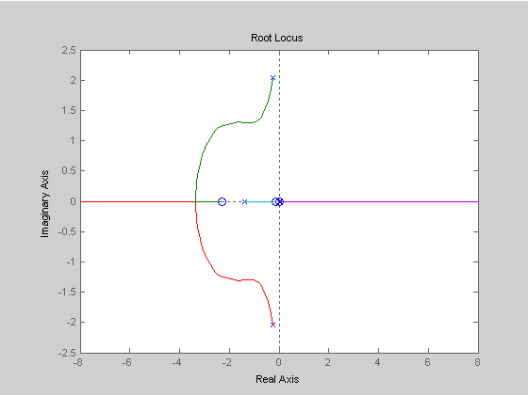

Figure 7 : Root Locus of Longitudinal Motion for AR = 7

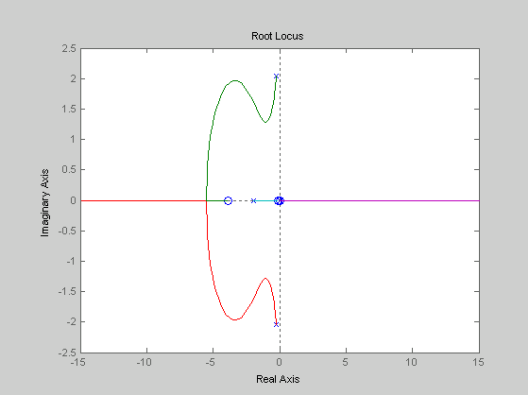

Figure 8 : Root Locus of Longitudinal Motion for AR = 8

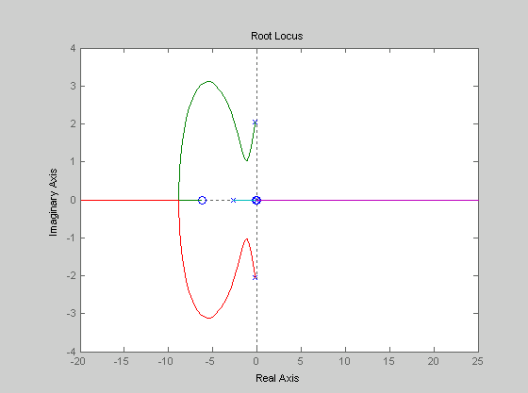

Figure 9 : Root Locus of Longitudinal Motion for AR = 9

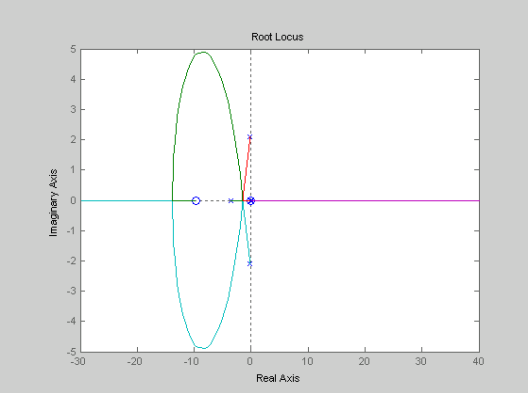

Figure 10 : Root Locus of Longitudinal Motion for AR = 10

CONCLUSION

This paper studies the viability of the variable aspect ratio wing application in terms of stability of the longitudinal and lateral motion. Preliminary study on the stability of the motion shows that it is feasible to apply the morphing wing on UAVs because the longitudinal and lateral motion remains stable for values of aspect ratio ranging from 3 to 10. All the poles are negative except for the spiral mode pole. However, this problem can be overcome by increasing the dihedral effect and yaw damping to make the spiral mode more stable. Future work can be done in improving the performance specifications by adding some form of compensation to the control design. It will also be interesting to analyze the effect of aspect ratios on aerodynamics, structure and aeroelastic properties.

ACKNOWLEDGMENT

The author would like to thank the Universiti Putra Malaysia's New Lecturer Research Scheme for supporting this research project.

REFERENCES

1. Blondeau, J. E. and Pines, D. J. (2004) Pneumatic Morphing Aspect Ratio Wing. AIAA 2004-1808, 45th AIAA/ASME/ASCE/ AHS/ ASC Structures, Structural Dynamics & Materials Conference, Palm Springs, California.
2. Henry, J. J., Blondeau, J. E. and Pines, D. J. (2005) Stability Analysis for UAVs with a Variable Aspect Ratio Wing. AIAA 2005-2044, 46th AIAA/ASME/ASCE/ AHS/ ASC Structures, Structural Dynamics & Materials Conference, Austin, Texas.

3. Torres, G. E. and Mueller, T. J. (2004) Low-Aspect-Ratio Wing Aerodynamics at Low Reynolds Number. AIAA Journal, Vol. 42, No. 5, 865-873.
4. Pelletier, A. and Mueller, T. J. (2000) Low Reynolds Number Aerodynamics of Low-Aspect-Ratio, Thin/Flat/Cambered-Plate Wings. Journal of Aircraft, Vol. 37, No. 5, 825-832.
5. Davidson, J. B., Chwalowski, P. and Lazos, B. S. (2003) Flight Dynamic Simulation Assessment of a Morphable Hyper-Elliptic Cambered Span Winged Configuration. AIAA 2003-5301, AIAA Atmospheric Flight Mechanics Conference and Exhibit, Austin, Texas.
6. Foster, T. M. and Bowman, W. J. (2005) Dynamic Stability and Handling Qualities of Small Unmanned-Aerial-Vehicles. AIAA 2005-1023, 43rd AIAA Aerospace Sciences Meeting and Exhibit, Reno, Nevada.
7. Hsiao, F. B. Hsieh, M. J., Lee, M. T., Chang, W. Y., Chien, Y. H., Liu, T. L. and Hsieh, S. H. (2005) The Simulation of Unmanned Aerial Vehicle Stability Under Atmospheric Conditions", 20th Bristol UAV Systems Conference.
8. Nelson, R. C. (1998) Flight Stability and Automatic Control. 2nd Edition, McGraw Hill, Singapore.

NOMENCLATURE

α	angle of attack
β	sideslip angle
δ	elevator angle
δ_a	aileron deflection
δ_r	rudder deflection
δ_T	throttle setting
Δ	increment of a parameter
η	control vector
θ	pitch angle
λ	root of characteristic equation
ζ	damping ratio
τ	roll time constant
ϕ	bank angle
ω_n	undamped natural frequency
AR	aspect ratio
g	gravitational acceleration
L/D	lift to drag ratio
L_β	rolling moment due to sideslip angle
L_{δ_α}	rolling moment due to change in aileron deflection
L_{δ_r}	rolling moment due to change in rudder deflection
L_p	rolling moment due to roll rate
L_r	rolling moment due to yaw rate
L_v	rolling moment due to velocity component in y direction
M_α	pitching moment due to angle of attack
M_{δ_T}	pitching moment due to change in throttle setting
M_q	pitching moment due to pitch rate
M_u	pitching moment due to velocity component in x direction

M_w pitching moment due to velocity component in z direction

$M_{\dot{w}}$ pitching moment due to change in velocity component in z direction

N_β yawing moment due to sideslip angle

N_{δ_a} yawing moment due to change in aileron deflection

N_p yawing moment due to roll rate

N_r yawing moment due to yaw rate

N_v yawing moment due to velocity component in y direction

p roll rate

q pitch rate

r yaw rate

u velocity component in x direction

u_0 refererence velocity component in x direction

UAV Unmanned Aerial Vehicle

Δw change in velocity component in z direction

x state vector

X_δ axial force due to change in elevator angle

X_{δ_T} axial force due to change in throttle setting

X_u axial force due to velocity component in x direction

X_w axial force due to velocity component in z direction

Y_β side force due to sideslip angle

Y_{δ_r} side force due to change in rudder deflection

Y_p side force due to roll rate

Y_r side force due to yaw rate

Y_v side force due to velocity component in y direction

Z_α normal force due to angle of attack

Z_δ normal force due to change in elevator angle

Z_{δ_T} normal force due to change in throttle setting

Z_q normal force due to pitch rate

Z_u normal force due to velocity component in x direction

Z_w normal force due to velocity component in z direction

$Z_{\dot{w}}$ normal force due to change in velocity component in z direction